Electronic Supplementary Material (ESI) for Soft Matter.

Non-monotonic temperature response of polymer mediated interactions

Fei Xie*, Clifford E. Woodward** and Jan Forsman**

*Theoretical Chemistry, P.O.Box 124, S-221 00 Lund, Sweden

**University College, University of New South Wales, ADFA Canberra ACT 2600, Australia

E-mail: fei.xie@teokem.lu.se

Supporting Information

Response of polymer mediated surface interactions to changes of the adsorption strength

Here we will illustrate how a gradual increase of the surface affinity (from a low level), leads to a surface interaction that is attractive for depleting surfaces, repulsive or nearly vanishing for intermediate affinities, and finally attractive for strongly adsorbing surfaces. This seems to be a very general response. We will consider simpler systems than those studied in the main paper, and all monomers are in the same state. Furthermore, the solvent is here completely implicit, only influencing the effective potential of mean force that acts between monomers. Specifically, we will consider two different models: ideal chains, with point-like monomers (theta solvent), and polymers composed of hard-sphere monomers (good solvent).

We will still use a model with two hard and infinite planar walls, located at $z = 0$ and $z = h$. As in the main text, the hard-wall potential serves to confine the monomers to the regime $0 < z < h$,

*To whom correspondence should be addressed

and infinite elsewhere. However, we will here also include short-ranged soft interaction, $W(z,h)$, acting on all monomers, with $W(z,h) = w(z) + w(h-z)$, and $\beta w(z) = A(1-z/z_c)^2$, $z < z_c$. For a given choice of z_c, we are thus left with a single adsorption parameter, A, describing the surface affinity. The temperature is kept constant.

Point-like monomers (theta solvent)

It should be emphasized that for this model, the density functional theory (DFT) is *exact*. We will simply illustrate the transition regime for two different degrees of polymerization, r. Here, we have set $z_c = 2b$, where b is the (fixed) bond length. In Figure 1 we see that the qualitative response is independent of chain length, but the range of A values for which the net interaction is repulsive does depend (slightly) on r. As expected, the response is more dramatic for longer chains, and the transition regime is more narrow (in terms of A values). Still, in both cases, the transition does in

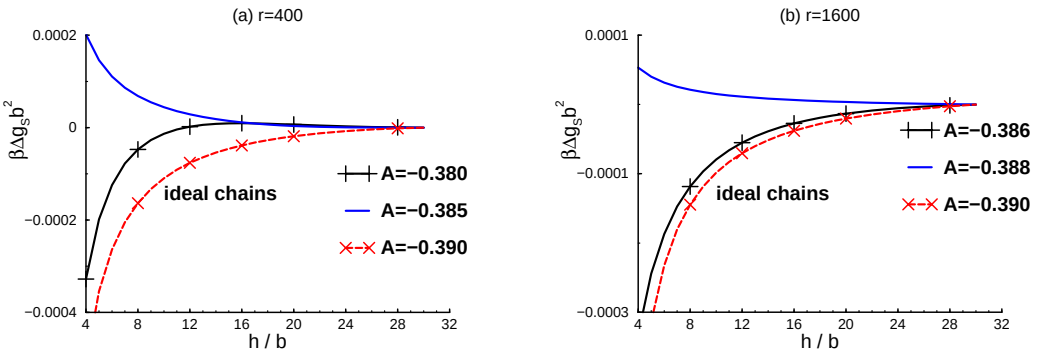

Figure 1: Net surface interaction free energies for ideal polymers, at various surface affinities. Note that we have neglected residual interactions beyond $h = 30b$, i.e. we have set $\Delta g_s(h) \approx g_s(h) - g_s(h = 30b)$.

both cases correspond to a remarkably small temperature change.

The ideal polymer model is useful, not only because the DFT predictions are exact. Another advantage is that the data is unusually easy to interpret, since the net outcome results from a rather limited set of contributions. For instance, given the short range of our surface potentials, there are only two separate contributions to the total pressure acting across the mid plane of the slit (i.e. the total internal pressure), namely repulsive ideal entropic term, P_{id} and an attractive bridging

pressure, P_{br}. The former is proportional to the monomer density at the mid plane, $n_m(h/2)$. More relevant to the net pressure is how these vary relative to their corresponding values in the bulk, i.e. $\Delta P_{id} \equiv P_{id} - P_{id}(h- > \infty)$ and $\Delta P_{br} \equiv P_{id} - P_{br}(h- > \infty)$. These quantities are plotted, across the

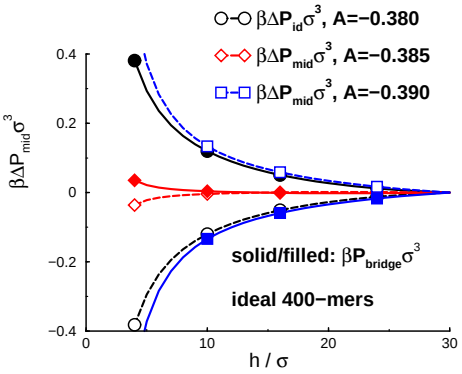

Figure 2: Net pressure contributions across the mid plane, for the systems with ideal 400-mers (graph (a) of Figure 1).

transition regime from depletion to bridging, in Figure 2. One anticipates that ΔP_{id} will be negative for weak surface potential, and positive for strong surface affinities, with an opposite trend for ΔP_{br}. In both extremes, the net attractive contribution dominates. In the transition between these, the outcome is less obvious. We recall that we observe a net repulsive interaction for a surface potential amplitude $A = -0.385$. In Figure 2, we see that ΔP_{br} and ΔP_{id} are repulsive and attractive, respectively, for this surface affinity. Hence, the net repulsive bridging pressure dominates, in this case.

Hard-sphere monomers (good solvent)

Here we consider polymers in which the monomers carry a hard sphere diameter $d = \sigma$. The excluded volume contribution is estimated via a "Generalized Flory-Dimer" theory.[1,2] The DFT is now in principle approximate, but numerous direct comparisons with simulation data have demonstrated that structural as well as thermodynamic predictions are remarkably accurate.[3,4] We will include calculations of 1600-mers as well as predictions for infinite chains. In the latter case, we use a reformulated version of polymer DFT, as described in an earlier work.[5] The range of the

surface potential is limited to $z_c = 2\sigma$, and the bond length is $b = 2\sigma$. We will consider two different bulk monomer densities, n_m^b. In Figure 3 we again observe a non-monotonic response to surface affinity. Though difficult to discern at this scale, the net interaction is weakly repulsive for 1600-mers, at the intermediate surface affinity ($\beta A = -0.94$), with an oscillatory regime at short range. With infinite chains, the interaction at long range is negligible.

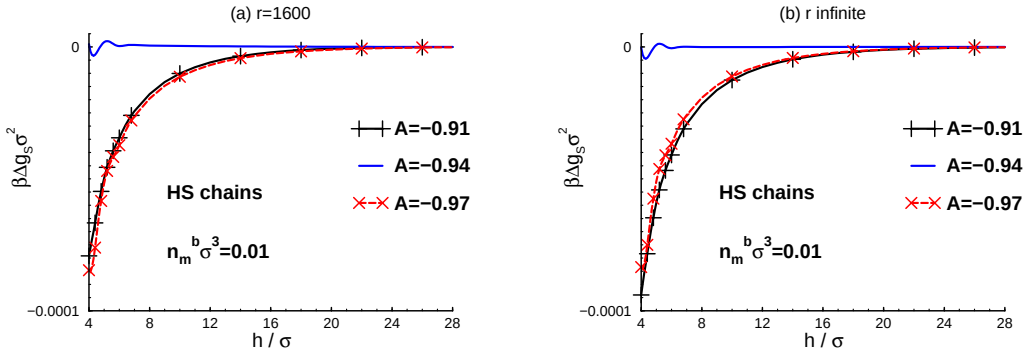

Figure 3: Net surface interaction free energies for polymers composed of herd-sphere monomers (good solvent, at various surface affinities. The bulk monomer concentration is $n_m^b \sigma^3 = 0.01$.

At a higher bulk density, the interactions are overall more short-ranged as expected. Still, the non-monotonic response is there, i.e. in a range of intermediate surface potentials, the interaction

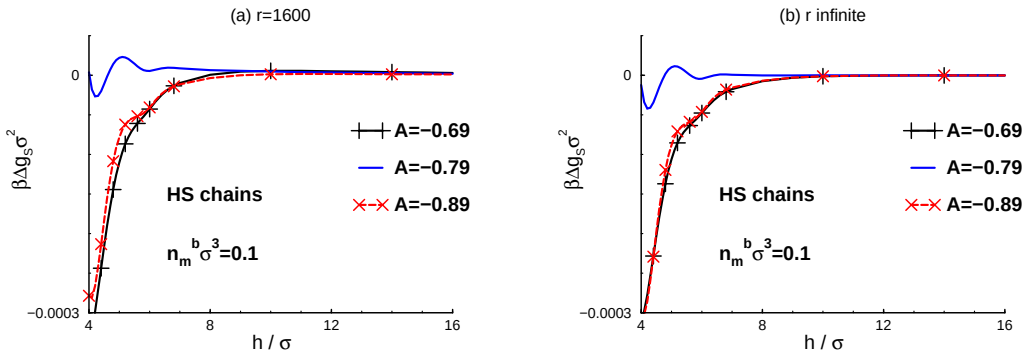

Figure 4: Net surface interaction free energies for polymers composed of herd-sphere monomers (good solvent, at various surface affinities. The bulk monomer concentration is $n_m^b \sigma^3 = 0.1$.

is either weakly repulsive, or vanishing, with some oscillations at short separations.

Polymer length dependence (main paper system)

Here, we simply show temperature response at the intermediate concentration $n_m^b\sigma^3 = 0.07$ with $g_B/g_A = 12$, in the main paper model system, but with $r = 400$. This is summarized in Figure 5, where we note that the overall behaviour is quite insensitive to the degree of polymerization.

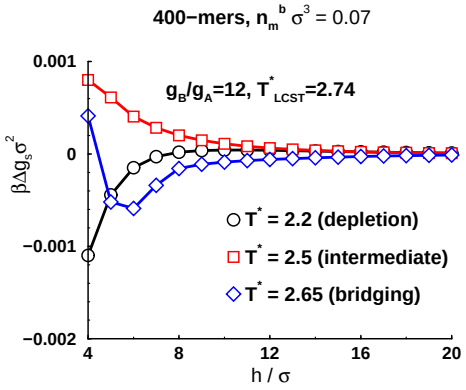

Figure 5: Net interaction free energies, at various temperatures, for the same system as in the main text (at $n_m^b\sigma^3 = 0.07$ and with $g_B/g_A = 12$), but with $r = 400$.

Thermodynamic consistency (main paper system)

Here, we show that our functional is thermodynamically consistent, in the sense that the forces acting across the right wall (say), as evaluated by the analytic derivative $-\partial\Delta\Omega/\partial h$, agrees with the corresponding discrete derivative, $-\delta\Delta\Omega/\delta h$. This can be seen as a generalization of the well-known "contact value theorem", CVT. Obviously, the CVT is an important thermodynamic consistency relation, and the two quantities should in principle agree. However, upon numerical functional minimization, space is naturally discretized, in the z dimension. We shall denote the grid spacing δz. For large choices of δz one can anticipate numerical deviations from the CVT. This is illustrated in Figure 6, where we see how the two methods to evaluate the net pressure gradually converge as δz becomes smaller. We also note, especially in graph (f), how $-\delta\Delta\Omega/\delta h$ converges much faster than the direct pressure evaluation. In other words, as long as we focus on free energies, and their derivatives, we do not have to use a finely spaced grid for our calculations.

In the main paper, we have set $\delta z = 0.05\sigma$ in all our calculations.

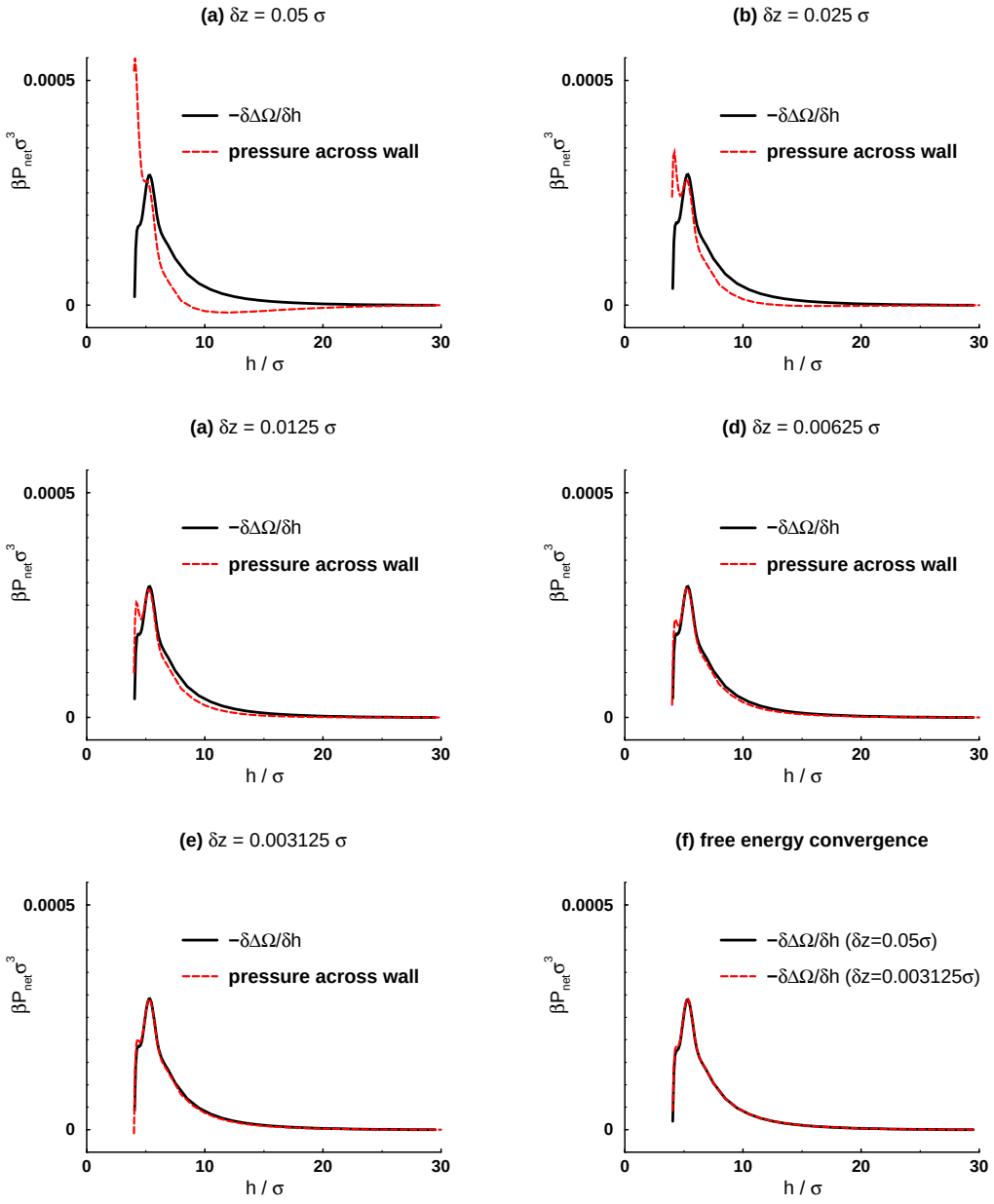

Figure 6: Net pressure, as evaluated analytically from $P_{wall} \equiv -\partial\Delta\Omega/\partial h$, and as a discrete derivative $-\delta\Delta\Omega/\delta h$, respectively, for various choices of grid spacing δz, used in the numerical calculations. This is the "intermediate temperature" ($T^* = 2.4$) studied in the main text, at $n_m^b\sigma^3 = 0.1$, with $g_B/g_A = 12$.
(a) $\delta z = 0.05\sigma$
(b) $\delta z = 0.025\sigma$
(c) $\delta z = 0.0125\sigma$
(d) $\delta z = 0.00625\sigma$
(e) $\delta z = 0.003125\sigma$
(f) Here, we compare predictions from $-\delta\Delta\Omega/\delta h$, as obtained with $\delta z = 0.05\sigma$ and $\delta z = 0.003125\sigma$, respectively.

Variation of LCST with polymer length (main paper systems)

As mentioned in the main text, both our investigated systems, i.e. $g_B/g_A = 12$ and $g_B/g_A = 13$, display a lower critical solution temperature, T^*_{LCST}. This temperature varies with polymer length, as illustrated in Figure 7. Note how demixing is present also for 45-mers, when $g_B/g_A = 13$, in

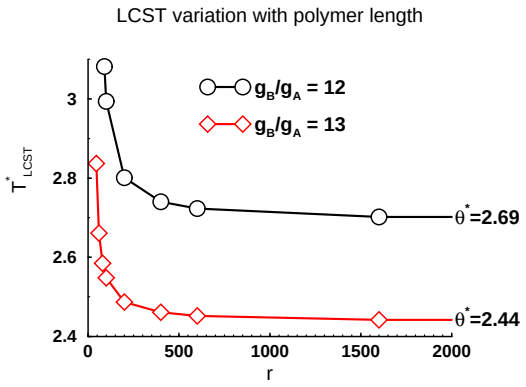

Figure 7: Variation of the LCST (or, T^*_{LCST}, in reduced units) with polymer length (r), for our two model systems in the main paper ($g_B/g_A = 12$ and $g_B/g_A = 13$).

agreement with experimental data[6] (but not when $g_B/g_A = 12$).

Variation of polymer size with temperature (mai paper system)

As we are using a mean-field theory, the concept of polymer size is not straigtforward to measure. Nevertheless, we have constructed a simple model that we believe does provide some information on polymer size, and its relative variation with temperature. Specifically, we consider a spherically symmetric system, where a polymer is grafted at one end, to the origin. The grafting extends one bond length, but is otherwise completely flexible, i.e. one of the end monomers in the chain is constrained to be within a sphere of radius b, centred at the origin: $4\pi \int_0^b r^2 n_g(r) dr = 1$ where $n_g(r)$ is the density of the grafted monomer at a distance r from the origin. Then we minimize the free energy of this system, at various reduced temperatures T^*. We use $< r >$ as our measure of "polymer size", with

$$< r >= \frac{\int_0^\infty r^3 n_m(r) dr}{\int_0^\infty r^2 n_m(r) dr} \tag{1}$$

The result, for our 45-mers with $g_B/g_A = 13$, in the relevant temperature regime $2.0 \leq T^* \leq$

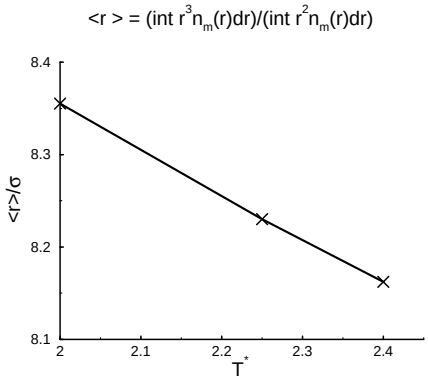

Figure 8: Variation of $< r >$ with temperature.

2.4, is shown in Figure 8. We note that the temperature dependence is weak, in agreement with experimental data.[7]

Capillary induced phase separation at bulk supercritical conditions

In this section, we will scrutinize the behaviour of the $g_B/g_A = 13$ system, at temperatures below, but rather close to, the LCST. As we have shown in an earlier work,[8] these systems may undergo a capillary induced phase separation (CIPS) even at temperatures below the LCST, i.e. even though the bulk is homogeneous for all compositions. This is indeed what we find, as illustrated in Figure 9, where we trace the grand potential for the concentrated and dilute branches separately. The steep slope of the concentrated branch leads to a rapid drop of the grand potential at separations below concentrated-dilute coexistence, i.e. below the separations that are denoted "CIPS" in the graphs.

References

(1) Honnell, K. G.; Hall, C. K. *J. Chem. Phys.* **1991**, *95*, 4481.

(2) Woodward, C. E.; Yethiraj, A. *J. Chem. Phys.* **1994**, *100*, 3181.

(3) Forsman, J.; Woodward, C. E. *J. Chem. Phys.* **2004**, *120*, 506.

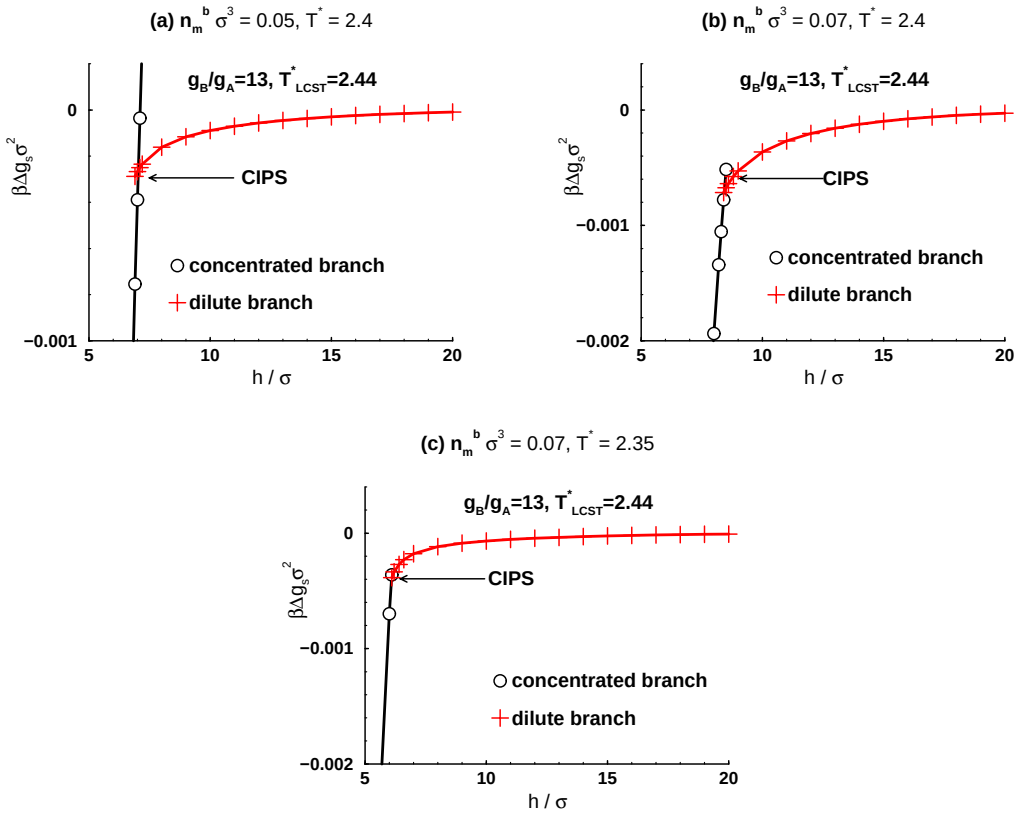

Figure 9: First-order capillary-induced phase transitions, CIPS, illustrated via the grand potential curves for the separate concentrated and dilute branches. These meet at a point of coexistence, which is indicated by "CIPS". The reduced lower critical solution temperature in the bulk is $T^* \approx 2.44$, so in all cases shown, the bulk is homogeneous for all compositions (no demixing).
(a) $T^* = 2.4$, $n_m^b \sigma^3 = 0.05$.
(b) $T^* = 2.4$, $n_m^b \sigma^3 = 0.07$.
(c) $T^* = 2.35$, $n_m^b \sigma^3 = 0.07$.

(4) Turesson, M.; Forsman, J.; Åkesson, T. *Phys. Rev. E* **2007**, *76*, 021801.

(5) Woodward, C. E.; Forsman, J. *Phys. Rev. E* **2006**, *74*, 010801.

(6) Saeki, S.; Kuwahara, N.; Nakata, M.; Kaneko, M. *Polymer* **1976**, *17*, 685 – 689.

(7) Branca, C.; MagazÃź, S.; Maisano, G.; Migliardo, F.; Migliardo, P.; Romeo, G. *Physica Scripta* **2003**, *67*, 551.

(8) Xie, F.; Woodward, C. E.; Forsman, J. *Langmuir* **2013**, *29*, 2659–2666.